

Topological magnons in a collinear altermagnet

Meng-Han Zhang,¹ Lu Xiao,¹ and Dao-Xin Yao^{1,*}

¹Guangdong Provincial Key Laboratory of Magnetoelectric Physics and Devices, State Key Laboratory of Optoelectronic Materials and Technologies, Center for Neutron Science and Technology, School of Physics, Sun Yat-Sen University, Guangzhou, 510275, China
(Dated: July 29, 2024)

We propose a model with Weyl magnons and weak topological magnons (\mathbb{Z}_2) in a collinear altermagnet on the honeycomb lattice. Altermagnetic magnon bands can be realized by breaking the symmetry of the second nearest neighbor exchange couplings without the Dzyaloshinskii-Moriya (DM) interaction. Besides the Chern number and \mathbb{Z}_2 invariant, chirality is important to describe the band topology. The model shows the nonzero magnon Nernst effect for both the strong and weak topological phases when a longitudinal temperature gradient exists. Furthermore, we find the orbital angular momentum induced purely by the topology of magnons, which can be probed by the Einstein-de Haas effect.

Introduction.- Magnons have been shown to facilitate spin transport with low-energy consumption[1, 2], which make them highly promising for the development of next-generation spintronic devices[3, 4]. Requiring low power, topological magnons can potentially be operated at ultra-high speeds in the context of the magnon Hall effect and the spin Nernst effect (SNE)[5, 6]. As two opposite copies of the magnon Hall effect for each spin species, the SNE provides valuable insights for understanding and manipulating magnon transport and related magnon dynamics[7, 8]. In geometrically frustrated honeycomb lattice, $\text{Ba}_3\text{CuSb}_2\text{O}_9$ gives rise to the magnon Hall effect in the absence of Dzyaloshinskii-Moriya interaction (DMI)[9–11], which highlights the complex magnetic ordering and unique spin excitations in this material rather than the typically DMI-induced Berry phase[12]. The magnon SNE and Berry curvature can be realized by the Heisenberg exchanges and the altermagnetic geometry. We investigate the magnon SNE in a honeycomb altermagnet and calculate the topological angular momentum of magnons manifesting even without the DMI.

In collinear altermagnets, magnons exhibit unique topological responses with symmetry-compensated zero net magnetization[13, 14]. Under the combined symmetry of mirror and time reversal[15], the altermagnets provide another mechanism to split the degenerate magnon bands distinct from DMI[16, 17]. The chiral edge modes contribute the transverse spin current suggesting that the altermagnets can potentially be used as effective spin generators for both spin orientations in the same device[18–20]. Recently, the altermagnetic metal RuO_2 maintaining non-degenerate chirality predicts valuable insights into the transport properties of the topological magnon current[21].

The classical Einstein-de Haas (EdH) effect encompasses the transfer of angular momentum based on the concept of conservation of angular momentum and its subsequent conversion into rotational kinetic energy [22]. The revelation of gyromagnetism has unveiled that the

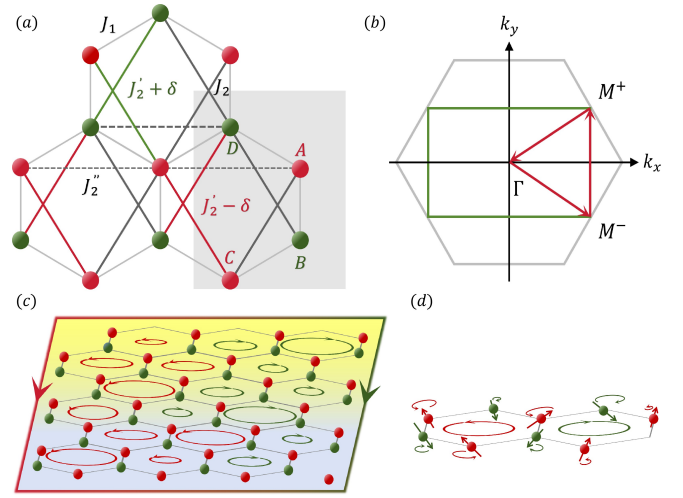


FIG. 1. (a) Altermagnet on the honeycomb lattice in magnetic Néel order with shaded region that represent the unit cell. (b) Brillouin zones (BZ) for the lattice (grey) and magnetic structure (green). (c) Schematics of the spin Nernst effect inducing magnon currents in transverse direction. (d) Magnon spin and angular momentum consisting of left-hand (red) chirality and right-hand (green) chirality.

source of magnetism stems from the inherent angular momentum possessed by electrons [23, 24]. Thus, the EdH effect offers a more precise means of accurately measuring the rotational motion by determining the gyromagnetic ratio [25–27]. Thus, the presence of Berry curvature can be seen as an equivalent magnetic field in momentum space[28–30]. Triggered by altermagnetic magnons, we demonstrate the EdH effect on the honeycomb altermagnets via theoretically calculating the differential gyromagnetic ratios.

In this Letter, we study the topological magnons in collinear honeycomb altermagnet. The manifestation of topological EdH effect occurs attributed to the presence of nontrivial chiral spin textures[31, 32]. We provide

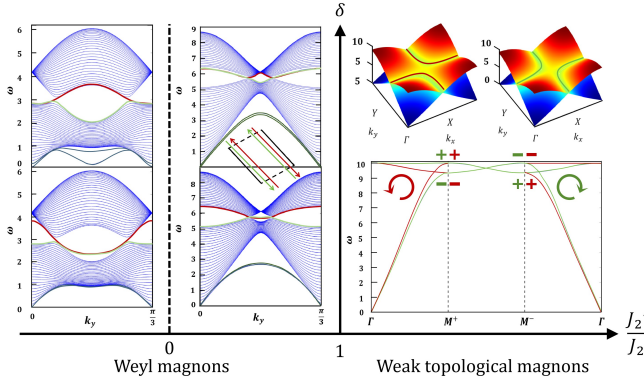


FIG. 2. Phase diagram of magnons in the $(J'_2/J_2, \delta)$ plane. Weyl magnons and weak topological magnons are separated by $J'_2/J_2 = 1$. In the weak topological magnon phase, the magnon bands show chiral nodal lines indicated by the circle arrows and red/green color. The inset shows the magnon currents along the opposite chiral edge modes.

theoretical investigation on the finite Hall response for further understanding the transport mechanisms[33–35], which provides a new way towards the high-speed and altermagnetic spintronic devices[36–38].

Model and method.— We construct a Heisenberg model on the honeycomb lattice with the Néel order shown in Fig. 1

$$H = J_1 \sum_{\langle mn \rangle} \mathbf{S}_m \cdot \mathbf{S}_n - (J_2, J'_2 \pm \delta, J''_2) \sum_{\langle\langle mn \rangle\rangle} \mathbf{S}_m \cdot \mathbf{S}_n, \quad (1)$$

where $J_1 > 0$ is the nearest neighbor coupling and $J_2, J'_2 \pm \delta$ and $J''_2 > 0$ represent three types of next-nearest neighbor couplings, which host the altermagnetic magnon bands via breaking the symmetry of sublattices.

Using the Fourier transform, we find the kernel matrix $H = \sum_{\mathbf{k}} \psi_{\mathbf{k}}^\dagger H_{\mathbf{k}} \psi_{\mathbf{k}}$ with

$$\begin{aligned} H_{\mathbf{k}} = & S\sigma_0 \otimes (h_0\tau_0 - f_1(\mathbf{k})\tau_+ - f_1^\dagger(\mathbf{k})\tau_-) \\ & - S\sigma_+ \otimes (f_2(\mathbf{k})\tau_+ + f_2^\dagger(\mathbf{k})\tau_- + g_\chi(\mathbf{k})\tau_+^0 + g_\chi(\mathbf{k})\tau_-^0) \\ & - S\sigma_- \otimes (f_2(\mathbf{k})\tau_+ + f_2^\dagger(\mathbf{k})\tau_- + g_\chi^\dagger(\mathbf{k})\tau_+^0 + g_\chi^\dagger(\mathbf{k})\tau_-^0). \end{aligned} \quad (2)$$

Here $\chi = \langle 0 | \Psi_{\mathbf{k}} \mathbf{S}^z \Psi_{\mathbf{k}}^\dagger | 0 \rangle = \pm 1$ denotes the left(right)-hand chirality of magnon bands as shown in the subfigure (c) and (d) of Fig. 1. The σ (spin part) and τ (chirality part) are identity matrix and Pauli matrices, $\sigma_\pm = \frac{1}{2}(\sigma_x \pm i\sigma_y)$ and $\sigma_\pm^0 = \frac{1}{2}(\sigma_0 \pm \sigma_z)$. Preserving the bosonic commutation relation $U^\dagger(\sigma_0 \otimes \tau_z)U = \sigma_0 \otimes \tau_z$, we introduce a para-

unitary matrix U to diagonalize the Hamiltonian $H_{\mathbf{k}}$

$$\begin{aligned} U \equiv & \sigma_0 \otimes \begin{bmatrix} \cosh \frac{\vartheta}{2} & -\sinh \frac{\vartheta}{2} e^{-i\varphi} \\ -\sinh \frac{\vartheta}{2} e^{i\varphi} & \cosh \frac{\vartheta}{2} \end{bmatrix} \\ & + \sigma_+ \otimes \begin{bmatrix} \cosh \frac{\theta}{2} e^{i\zeta} & -\sinh \frac{\theta}{2} e^{-i\phi} \\ -\sinh \frac{\theta}{2} e^{i\phi} & \cosh \frac{\theta}{2} e^{i\zeta} \end{bmatrix} \\ & + \sigma_- \otimes \begin{bmatrix} \cosh \frac{\theta}{2} e^{-i\zeta} & -\sinh \frac{\theta}{2} e^{-i\phi} \\ -\sinh \frac{\theta}{2} e^{i\phi} & \cosh \frac{\theta}{2} e^{-i\zeta} \end{bmatrix}. \end{aligned} \quad (3)$$

The magnon bands of the model can be obtained analytically as

$$\hbar\omega_\chi^\pm = S\sqrt{\Lambda(\mathbf{k}) \pm \lambda(\mathbf{k})}, \quad (4)$$

where the $+(-)$ sign corresponds to the acoustical (optical) branch, $\Lambda(\mathbf{k})$ and $\lambda(\mathbf{k})$ are related functions constructed by $h_0, f_1(\mathbf{k}), f_2(\mathbf{k})$ and $g_\chi(\mathbf{k})$, where typical energy bands are shown in Fig. 2.

Using a hyperbolic parameterization l and ℓ for Eq. (4), we can rewrite the magnon bands as $\hbar\omega_\chi^\pm = \sqrt{l^2 + \ell^2 \pm 2l\ell(\cosh \theta \cosh \vartheta + \sinh \theta \sinh \vartheta \cos(\phi - \varphi))}$, where $g_\chi(\mathbf{k}) = l \cosh \theta e^{i\zeta}$. Around the linear band crossings (Weyl points), the topological dynamics can be obtained by taking the Berry curvature that gives rise to a transverse motion of the magnon wave packet

$$\begin{aligned} \Omega_n = & -\text{Im} \langle \nabla \Psi_{\mathbf{k}} | \times (\sigma_0 \otimes \tau_z) | \nabla \Psi_{\mathbf{k}} \rangle \\ = & \frac{\sinh \theta}{2} \nabla \theta \times \nabla \phi + \frac{\sinh \vartheta}{2} \nabla \vartheta \times (\nabla \phi + \nabla \zeta). \end{aligned} \quad (5)$$

At the time-reversal-invariant momenta points Γ_i , Hamiltonian satisfies the inversion symmetry $\mathbf{R}U\mathbf{H}_{\mathbf{k}}U\mathbf{H}_{-\mathbf{k}}\mathbf{R}=0$, where \mathbf{R} is the inversion operator defined as $\sigma_0 \otimes (\tau_+ + \tau_-)$. The corresponding eigenvalues of \mathbf{R} are $\xi_n(\Gamma_i)$ and the eigenvectors of $\sigma_0 \otimes \tau_z H_{\mathbf{k}}$ are $\Psi^\dagger(\Gamma_i) = [\cosh \frac{\theta}{2}(\Gamma_i), -\sinh \frac{\theta}{2}(\Gamma_i)e^{-i\phi(\Gamma_i)}, -\cosh \frac{\vartheta}{2}(\Gamma_i)e^{i\zeta}, -\sinh \frac{\vartheta}{2}(\Gamma_i)e^{-i\varphi(\Gamma_i)}]$. Hence, the topological protection for the weak topology is characterized by $(-1)^{\nu_n} = \prod_n \xi_n(\Gamma_i)$.

We further analyze the combined symmetry of \mathbf{R} and the pseudo-time-reversal operator $\mathcal{T} = \sigma_z \otimes i\tau_y \mathcal{K}$, where \mathcal{K} denotes the complex conjugate operator. Taking into account this combined symmetry, a more practical form of ν_n is given by the \mathbb{Z}_2 invariant.

$$\nu_n = \frac{1}{2\pi} [\Upsilon_n - \iint_{\text{HalfBZ}} dk_x dk_y \Omega_n] \text{mod} 2, \quad (6)$$

where Υ_n is the Berry phase of the n th band, and Ω_n is the corresponding Berry curvature.

Weyl magnons and weak topology.— For the $J'_2 < J_2$ case with finite δ , the mirror symmetry M_x and rotation symmetry C_{6v} are broken. Pairs of Weyl points emerge at $W_\chi = (\frac{\chi}{\sqrt{3}} \arccos \eta, \frac{\chi}{3} \arccos \eta)$ with $\eta = \frac{-J_1^2 + 2h_0 J'_2}{J_1^2 - 2h_0 J_2}$ along the high symmetry axis Γ - M as shown in the subfigure

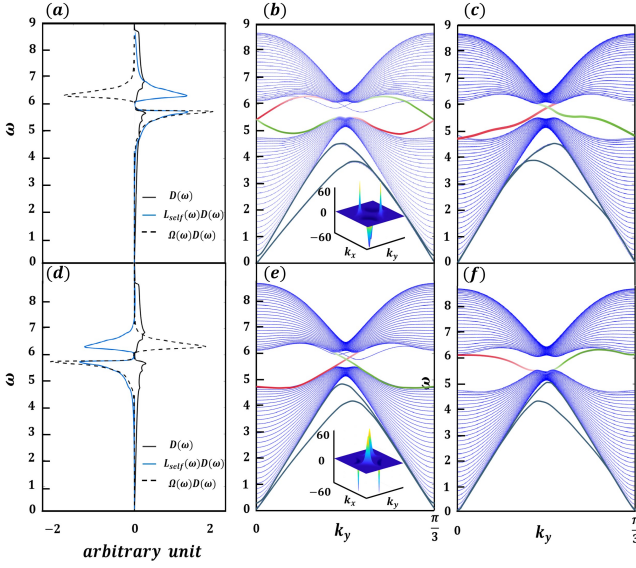


FIG. 3. Weyl magnons with $J_1=1$. (a), (b), (c) are the chiral edge modes, DOS $D(\omega)$, product density $\Omega(\omega)D(\omega)$ and angular momentum product density $L_{self}(\omega)D(\omega)$ for $J_2=0.8$, $\delta=0.4$ and $J_2=0.2$ respectively. (d), (e), (f) are the same quantities for $J_2=0.8$, $\delta=-0.4$ and $J_2=0.2$. The insets show the magnon Berry curvature at the two Weyl points.

(b) of Fig. 1. The Weyl magnons are given with the related functions

$$\begin{aligned}\Lambda(\mathbf{k}) &= h_0^2 - f_1(\mathbf{k})f_1^\dagger(\mathbf{k}) + g_\chi(\mathbf{k})g_\chi^\dagger(\mathbf{k}) - f_2(\mathbf{k})f_2^\dagger(\mathbf{k}), \\ \lambda(\mathbf{k}) &= \sqrt{\lambda_1^2(\mathbf{k}) + \lambda_2(\mathbf{k})},\end{aligned}\quad (7)$$

where $\lambda_1(\mathbf{k})=f_1(\mathbf{k})f_2^\dagger(\mathbf{k})+f_2(\mathbf{k})f_1^\dagger(\mathbf{k})+2h_0\text{Reg}_\chi(\mathbf{k})$, and $\lambda_2(\mathbf{k})=4\text{Im}g_\chi^2(\mathbf{k})[h_0^2-f_2(\mathbf{k})f_2^\dagger(\mathbf{k})]$. With the crossings residing at the $\lambda_1(\mathbf{k})=0$, we construct the effective Hamiltonian by introducing the projection operator $\mathbf{P}=U(\sigma_0 \otimes \tau_z)(U)^\dagger(\sigma_0 \otimes \tau_z)=(\sigma_0 \otimes \tau_z)U(\sigma_0 \otimes \tau_z)(U)^\dagger$. In the vicinity of W_χ , we expand the eigenvectors to the first order and project the Bose BdG Hamiltonian into the subspace.

$$\begin{aligned}H_{\mathbf{q}} &= \int d\mathbf{q}\Psi_{\mathbf{q}}^\dagger \begin{bmatrix} H_{eff}^{W_\chi} & 0 \\ 0 & H_{eff}^{W_\chi} \end{bmatrix} \Psi_{\mathbf{q}} \\ H_{eff}^{W_\chi} &= \sqrt{E_{W_\chi}}\sigma_0 + v_y q_x \sigma_y \pm v_x q_y \sigma_x \pm \frac{\Delta_{W_\chi}}{2}\sigma_z,\end{aligned}\quad (8)$$

where $E_{W_\chi}=h_0^2-3J_1^2-2J_2^2\eta+\frac{4(J_2-J_2')^2J_1^4}{(J_1^2-2h_0J_2)^2}$, v_x and v_y are the anisotropic velocities of magnons at the weyl points, where the specific form can be found in Appendix A.

We introduce the J_2' term as an operator $\mathbf{M}=\sigma_+^0 \otimes (M(\mathbf{k})\sigma_0)$ to create the mass of Weyl magnons. $M(\mathbf{k})=2J_2'[1-\cos(\mathbf{k}\cdot\mathbf{a}_1+\mathbf{k}\cdot\mathbf{a}_2)+\sin(\mathbf{k}\cdot\mathbf{a}_1+\mathbf{k}\cdot\mathbf{a}_2)]$ is the staggered coupling strength generating the topological gap Δ_{W_χ} . Thus the Berry connection is modified

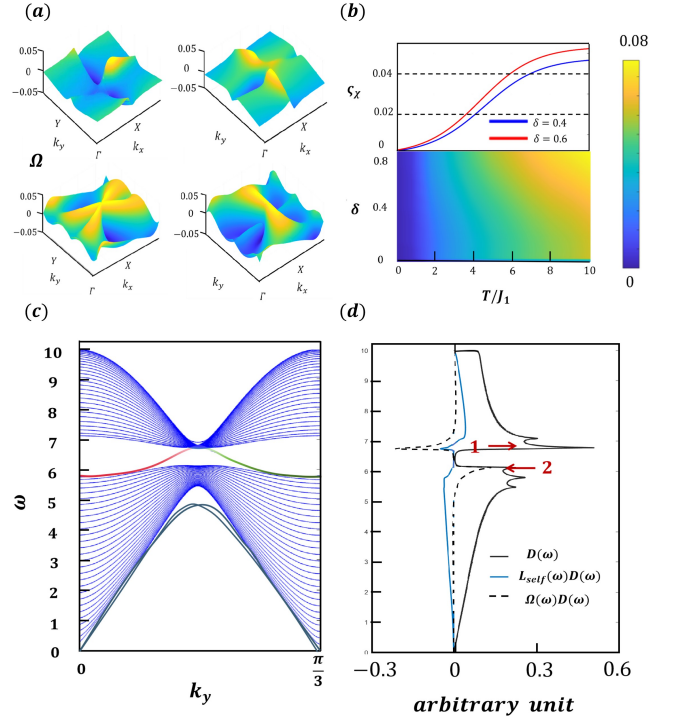


FIG. 4. Weak topological magnons with $J_1=1$. (a) Berry curvatures of the acoustical (optical) magnon bands with different chiralities. (b) The magnon spin Nernst conductivity as a distribution of temperature and δ . (c) Topological edge modes of the finite ribbon geometry with $J_2=1.2$ and $\delta=0.4$. (d) The $D(\omega)$, $\Omega(\omega)D(\omega)$ and $L_{self}(\omega)D(\omega)$ for the right-hand chirality, where the two von Hove singularities are marked.

with \mathbf{M} operator as $i[(\sigma_0 \otimes \tau_z)\mathbf{M}U^\dagger(\sigma_0 \otimes \tau_z)\nabla U]$, and the \mathbf{M} -Berry curvature is defined as

$$\Omega_n = \frac{\mathbf{d}\mathbf{q} \cdot [\partial_{q_x}\mathbf{d}\mathbf{q} \times \partial_{q_y}\mathbf{d}\mathbf{q}]}{|\mathbf{d}\mathbf{q}|^3}\quad (9)$$

where $\mathbf{d}\mathbf{q}=v_x\mathbf{q}_x+v_y\mathbf{q}_y+\frac{\Delta_{W_\chi}}{2}\mathbf{q}_z$ and $\Omega_n=\frac{\Delta_{W_\chi}}{2(v_xv_y)^{\frac{3}{2}}}$. Here, the effective mass m^* of Weyl magnons is described by the quadratic dispersion in the vicinity of energy valleys $\omega_{W_\chi}^\pm(q)\approx\sqrt{E_{W_\chi}}\pm c_\omega q^2$ (see Appendix A). As shown in Fig. 3, the Berry curvature is of the monopole type located at the Weyl points with the topological charge χ . The chiral edge state crossings are switched to $k_y=0$ and $k_y=\pi$ indicating the sign change of δ .

By contrast, the δ term opens a finite gap in weak topological phase when $J_2'>J_2$ as shown in Fig. 2. We further observe the annihilation of pairs of Weyl points and the nodal-lines touch at the M point forming a phase boundary when the condition $J_2'=J_2$ is satisfied. The gap Δ_δ is $S\sqrt{\Lambda_\delta}+\lambda_\delta-S\sqrt{\Lambda_\delta}-\lambda_\delta$ with $\Lambda_\delta=h_0^2-3J_1^2-\frac{2J_2^2}{|\eta|}+\frac{4(J_2-J_2')^2J_1^4}{\eta^2(J_1^2-2h_0J_2)^2}+\frac{4\delta^2(\eta^2-1)}{\eta^2}$ and $\lambda_\delta=\frac{2\delta\sqrt{\eta^2-1}}{|\eta|}\sqrt{h_0^2-2\frac{J_1^2(\eta+1)}{\eta}}$. The symmetry is characterized by a \mathbb{Z}_2 invariant in the absence of the \mathbf{M} opera-

tor, whereas the δ term can not break the the mirror symmetry M_x . Although the combined symmetry forbids the δ -gapped topology to have a nonzero Chern number, the Berry curvature can be nontrivial around the δ -induced topological gap with $\nu_n=1$ (see Fig. 4).

Topological responses.- Since the chiral magnons are completely decoupled, we obtain the magnon Hall current induced by temperature gradient ∇T [7].

$$\begin{aligned} \mathbf{J}_\chi^T &= \mathbf{z} \times \nabla T \sum_{n, \mathbf{k}} c_1[n_B(\mathbf{k})] \chi \Omega_n(\mathbf{k}), \\ &= \varsigma_\chi \mathbf{z} \times \nabla T, \end{aligned} \quad (10)$$

where $c_1[x]=(1+x)\ln(1+x)-x\ln x$, and $n_B(\mathbf{k})$ is the Bose-Einstein distribution. In the weak topological phase, an analytic estimate of the current conductivity at low temperatures is obtained as $\varsigma_\chi = \sum_n \int d\omega c_1[n_B(\omega)] \chi \Omega_n(\omega)$, where $\sum_n c_1[n_B(\omega)]$ is approximated as $c_\delta = \frac{\Delta^+ - \Delta^-}{2 \sinh \frac{\sqrt{\Lambda_\delta + \lambda_\delta}}{2k_B T} \sinh \frac{\sqrt{\Lambda_\delta - \lambda_\delta}}{2k_B T}}$ (details of Δ^+ and Δ^- are given in Appendix A). In the limit of $J_2'' \ll J_1$, the approximate expression of ς_χ generated by the \mathbf{M} operator of each Weyl point is given by

$$\begin{aligned} \varsigma_\chi &= \hbar \sum_n \int \frac{\sqrt{E_{W_\chi}}}{\sqrt{E_{W_\chi} - c_\omega q^2}} d\omega D(\omega) \chi \Omega_\chi(\omega) n_B(\omega) \\ &\simeq \frac{v_x v_y \Delta_{W_\chi}}{2\pi} c_\omega c_{\Delta_{W_\chi}} q^2, \end{aligned} \quad (11)$$

where $D(\omega)$ is the density of magnons, and $c_{\Delta_{W_\chi}} = \frac{\sinh \frac{\Delta_{W_\chi}}{2k_B T}}{-\cosh \frac{\sqrt{E_{W_\chi}}}{k_B T} + \cosh \frac{\Delta_{W_\chi}}{2k_B T}}$. We plot numerical results for the temperature and the δ strength dependence of the magnon Nernst conductivities in Fig. 4. The Berry curvature flips sign across two von Hove singularities in the DOS reflecting different chirality of magnon nodal lines.

Considering the validity of the semiclassical approach, the response of the topological angular momentum can be derived via the particle self-rotation operator and the current operator $\mathbf{L} = \mathbf{L}_{self} + \mathbf{L}_{edge}$ [39, 40].

$$\begin{aligned} \mathbf{L}_{self} &= m^* \text{Im} \sum_{n, \mathbf{k}} \langle \langle \nabla \Psi_k | \frac{n_B}{2k_B} (\omega_{n\mathbf{k}} - H) \chi | \nabla \Psi_k \rangle \rangle, \\ \mathbf{L}_{edge} &= m^* \text{Im} \sum_{n, \mathbf{k}} \langle \langle \nabla \Psi_k | [T c_1(n_B) - \frac{n_B \omega_{n\mathbf{k}}}{k_B}] \chi | \nabla \Psi_k \rangle \rangle \end{aligned} \quad (12)$$

Defining the sublattice magnetization $S_\uparrow = -S_\downarrow = \mathbf{S}^z$, we obtain the effective magnetic moment $m = S - \langle \Psi_k^\dagger \Psi_k \rangle = S - \sum_{n, \mathbf{k}} n_B(\omega_{n\mathbf{k}})$. To describe the EdH effect of topological magnons, we use the differential gyromagnetic ratios $\gamma_{self}^* = \frac{\partial \mathbf{L}_{self} / \partial T}{\partial (S - m) / \partial T}$ and $\gamma_{edge}^* = \frac{\partial \mathbf{L}_{edge} / \partial T}{\partial (S - m) / \partial T}$ to represent the

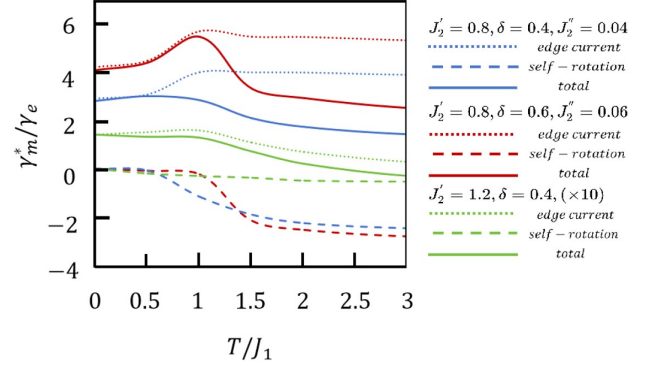


FIG. 5. Temperature dependence of the differential gyromagnetic ratio on the altermagnetic magnons with $J_1=1$ and $J_2=0.8$. Parameter choices are $\delta=0.4, 0.6$ for $J_2''=0.04, 0.06$ when $J_2'=0.8$ respectively, and $\delta=0.4$ for weak topological phase as $J_2'=1.2$.

pure geometric effect. They are calculated as

$$\begin{aligned} \gamma_{edge}^* &= m^* \frac{\sum_n \int d\omega (TD(\omega) - \omega) n_B(\omega) \chi \Omega_\chi(\omega) / \partial T}{\sum_n \int d\omega n_B(\omega) / \partial T}, \\ \gamma_{self}^* &= m^* \frac{\sum_n \int d\omega n_B(\omega) \chi \mathbf{L}_{self}(\omega)}{\sum_n \int d\omega n_B(\omega) / \partial T}. \end{aligned} \quad (13)$$

Numerical calculations of the differential gyromagnetic ratios are shown in Fig. 5. The whole bands contribute in additive way to the differential gyromagnetic ratio, which results in a much larger EdH effect[41, 42]. The high-energy edge states due to \mathbf{M} operator are chiral and are protected by the finite Chern number because of the non-trivial topology of the bulk magnons. These edge states are also expected to contribute to SNE conductivity in the finite geometry[43, 44].

Conclusion.- In summary, we have proposed a fundamental framework of chirality-driven magnon transport in a honeycomb altermagnet. By focusing on the weyl crossing, we have revealed that the interplay between the collinear altermagnet and the magnon Berry curvature results in a spin Hall current without the traditional DMI. The symmetry breaking of the second nearest neighbor exchange couplings are used to introduce Weyl magnons and \mathbb{Z}_2 topological magnons. A magnon Nernst effect exists in both the strong and weak topological phases. Finally we show that the model has a pure topological EdH effect, which can be used for mechanical detection and manipulation of the magnetic angular momentum in 2D altermagnets. Our study provides a new way to realize altermagnetic magnons and works as a building block for more sophisticated altermagnetic spintronics.

Acknowledgements.- We thank Zi-Jian Xiong for helpful discussions. This project is supported by NKRDP-

2022YFA1402802, NSFC-92165204, Leading Talent Program of Guangdong Special Projects (201626003), Guangdong Provincial Key Laboratory of Magnetoelectric Physics and Devices (No. 2022B1212010008), and Shenzhen Institute for Quantum Science and Engineering (No. SIQSE202102).

* yaodaox@mail.sysu.edu.cn

- [1] Y. Onose, T. Ideue, H. Katsura, Y. Shiomi, N. Nagaosa, and Y. Tokura, *Science* **329**, 297–299 (2010).
- [2] T. Ideue, Y. Onose, H. Katsura, Y. Shiomi, S. Ishiwata, N. Nagaosa, and Y. Tokura, (2012).
- [3] A. V. Chumak, V. I. Vasyuchka, A. A. Serga, and B. Hillebrands, *Nature Physics* **11** (2015).
- [4] M.-H. Zhang and D.-X. Yao, *Phys. Rev. B* **108**, 144407 (2023).
- [5] G. Go, D. An, H.-W. Lee, and S. K. Kim, *Nano Letters* **24**, 5968 (2024).
- [6] H. Hong, T. K., and H. Xiao, (2021), arXiv:2112.11652 [cond-mat.mes-hall].
- [7] V. A. Zyuzin and A. A. Kovalev, *Phys. Rev. Lett.* **117**, 217203 (2016).
- [8] R. Cheng, S. Okamoto, and D. Xiao, *Phys. Rev. Lett.* **117**, 217202 (2016).
- [9] K. Sugii, M. Shimozaawa, D. Watanabe, *et al.*, *Phys. Rev. Lett.* **118**, 145902 (2017).
- [10] I. Dzyaloshinsky, *J. Phys. Chem. Solids* **4**, 241 (1958).
- [11] T. Moriya, *Phys. Rev.* **120**, 91 (1960).
- [12] H. Y. Yuan, Y. Cao, A. Kamra, R. A. Duine, and P. Yan, *Physics Reports* **965**, 1 (2022).
- [13] R. M. Fernandes, V. S. de Carvalho, T. Birol, and R. G. Pereira, *Phys. Rev. B* **109**, 024404 (2024).
- [14] I. I. Mazin, *Phys. Rev. B* **107**, L100418 (2023).
- [15] D. Zhu, Z.-Y. Zhuang, Z. Wu, and Z. Yan, *Phys. Rev. B* **108**, 184505 (2023).
- [16] K. Parshukov, R. Wiedmann, and A. P. Schnyder, (2024), arXiv:2403.09520 [cond-mat.mes-hall].
- [17] Q. Cui, B. Zeng, T. Yu, H. Yang, and P. Cui, (2023), arXiv:2306.08976 [cond-mat.mes-hall].
- [18] Y. Hatsugai, *Phys. Rev. B* **48**, 11851 (1993).
- [19] A. Mook, J. Henk, and I. Mertig, *Phys. Rev. B* **90**, 024412 (2014).
- [20] L. Šmejkal, J. Sinova, and T. Jungwirth, *Phys. Rev. X* **12**, 031042 (2022).
- [21] L. Šmejkal, A. Marmodoro, Ahn, *et al.*, *Phys. Rev. Lett.* **131**, 256703 (2023).
- [22] A. Einstein and W. de Haas, *Series B Physical Sciences* **18**, 696 ((1915)).
- [23] J. Q. Stewart, *Phys. Rev.* **11**, 100 (1918).
- [24] S. J. Barnett, *Phys. Rev.* **6**, 239 (1915).
- [25] J. Li, T. Datta, and D. Yao, *Phys. Rev. Res.* **3**, 023248 (2021).
- [26] M.-H. Zhang and D.-X. Yao, *Phys. Rev. B* **107**, 024408 (2023).
- [27] D.-X. Yao and E. W. Carlson, *Phys. Rev. B* **78**, 052507 (2008).
- [28] L. Z. and Q. Niu, *Phys. Rev. Lett.* **112**, 085503 (2014).
- [29] E. M. Chudnovsky, R. Jaafar, and D. A. Garanin, *Phys. Rev. B* **79**, 104410 (2009).
- [30] A. Osada, A. Glloppe, Y. Nakamura, and K. Usami, *New J. Phys.* **20**, 103018 (2018).
- [31] J. Becker, A. Tsukamoto, A. Kirilyuk, J. C. Maan, T. Rasing, P. C. M. Christianen, and A. V. Kimel, *Phys. Rev. Lett.* **118**, 117203 (2017).
- [32] A. A. Kovalev, G. E. W. Bauer, and A. Brataas, *Phys. Rev. Lett.* **94**, 167201 (2005).
- [33] J. Tejada, R. D. Zysler, E. Molins, and E. M. Chudnovsky, *Phys. Rev. Lett.* **104**, 027202 (2010).
- [34] H. Keshtgar, S. Streib, A. Kamra, Y. M. Blanter, and G. E. W. Bauer, *Phys. Rev. B* **95**, 134447 (2017).
- [35] A. A. Kovalev, G. E. W. Bauer, and A. Brataas, *Phys. Rev. B* **75**, 014430 (2007).
- [36] M. Gohlke, A. Corticelli, R. Moessner, P. A. McClarty, and A. Mook, (2022), arXiv:2211.15157 [cond-mat.other].
- [37] C. R. W. Steward, R. M. Fernandes, and J. Schmalian, *Phys. Rev. B* **108**, 144418 (2023).
- [38] T. A. Maier and S. Okamoto, *Phys. Rev. B* **108**, L100402 (2023).
- [39] R. Matsumoto and S. Murakami, *Phys. Rev. Lett.* **106**, 197202 (2011).
- [40] R. Matsumoto and S. Murakami, *Phys. Rev. B* **84**, 184406 (2011).
- [41] J. H. Mentink, M. I. Katsnelson, and M. Limeshko, *Phys. Rev. B* **99**, 064428 (2019).
- [42] V. Baltz, A. Manchon, M. Tsai, T. Moriyama, T. Ono, and Y. Tserkovnyak, *Rev. Mod. Phys.* **90**, 015005 (2018).
- [43] Z. Feng, X. Zhou, L. Šmejkal, *et al.*, *Nature Electronics* **5**, 735 (2022).
- [44] X.-B. Chen, J. Ren, J.-Y. Li, Y.-T. Liu, and Q.-H. Liu, (2023), arXiv:2307.12366 [cond-mat.mtrl-sci].

Appendix A: Magnon dynamics

We use the Holstein-Primakoff (HP) representation to study the magnetic excitations of the model and set the length of the primitive vectors to be unity. The original spin Hamiltonian can be mapped to a bosonic model following the HP transformation:

$$\begin{aligned} \mathbf{S}_{m\alpha}^+ &= \sqrt{2S - \alpha_m^\dagger \alpha_m} \alpha_m, \quad \mathbf{S}_{m\alpha}^- = \alpha_m^\dagger \sqrt{2S - \alpha_m^\dagger \alpha_m}, \\ \mathbf{S}_{m\beta}^+ &= \beta_m^\dagger \sqrt{2S - \beta_m^\dagger \beta_m}, \quad \mathbf{S}_{m\beta}^- = \sqrt{2S - \beta_m^\dagger \beta_m} \beta_m, \\ \mathbf{S}_{m\alpha}^z &= S - \alpha_m^\dagger \alpha_m, \quad \mathbf{S}_{m\beta}^z = \beta_m^\dagger \beta_m - S. \end{aligned} \quad (\text{A-1})$$

where α_m^\dagger (α_m) is the bosonic magnon creation (annihilation) operator at site m . Subsequently, we perform the Fourier transformation using the definition

$$\alpha_{\mathbf{k}}^\dagger = \frac{1}{\sqrt{N}} \sum_m e^{i\mathbf{k}\cdot\mathbf{R}_m} \alpha_m^\dagger. \quad (\text{A-2})$$

Thus, the Hamiltonian is given in the reciprocal space by

$$\mathcal{H} = \sum_{\mathbf{k}} \psi_{\mathbf{k}}^\dagger H(\mathbf{k}) \psi_{\mathbf{k}}, \quad (\text{A-3})$$

where $\psi_{\mathbf{k}}^\dagger \equiv [\alpha_{1,\mathbf{k}}^\dagger, \beta_{2,-\mathbf{k}}, \alpha_{3,\mathbf{k}}^\dagger, \beta_{4,-\mathbf{k}}]$ expressing the Hamiltonian in the Nambu basis

$$H_{\mathbf{k}} = S \begin{bmatrix} A_{\mathbf{k}} & B_{\mathbf{k}} \\ B_{\mathbf{k}}^\dagger(\mathbf{k}) & A_{\mathbf{k}} \end{bmatrix}, \quad (\text{A-4})$$

with $A_{\mathbf{k}}$ is hermitian

$$\begin{bmatrix} h_0 & f_1(\mathbf{k}) \\ f_1^\dagger(\mathbf{k}) & h_0 \end{bmatrix}, \quad (\text{A-5})$$

and $B_{\mathbf{k}}$ is normal

$$\begin{bmatrix} g_\chi(\mathbf{k}) & f_2(\mathbf{k}) \\ f_2(\mathbf{k}) & g_\chi(\mathbf{k}) \end{bmatrix}. \quad (\text{A-6})$$

With the lattice vectors given by $\mathbf{a}_1 = (\frac{\sqrt{3}}{2}, \frac{1}{2})a$ and $\mathbf{a}_2 = (\frac{\sqrt{3}}{2}, \frac{1}{2})a$, we use $h_0 = 3J_1 + 2J_2 + 2J_2'$, $f_1(\mathbf{k}) = J_1 e^{i\mathbf{k} \cdot (-\mathbf{a}_1 + \mathbf{a}_2)}$, $f_2(\mathbf{k}) = J_1 e^{-i\mathbf{k} \cdot \mathbf{a}_1} + J_1 e^{i\mathbf{k} \cdot \mathbf{a}_2}$. We introduce the unitary matrix U that can diagonalize A , B and consequently $D \equiv A^2 - B^\dagger B$. The chirality of magnon bands depend on $g_1(\mathbf{k}) = 2J_2 \cos(-\mathbf{k} \cdot \mathbf{a}_1 + 2\mathbf{k} \cdot \mathbf{a}_2) + 2J_2' \cos(2\mathbf{k} \cdot \mathbf{a}_1 - \mathbf{k} \cdot \mathbf{a}_2) - 2i\delta \sin(2\mathbf{k} \cdot \mathbf{a}_1 - \mathbf{k} \cdot \mathbf{a}_2)$ and $g_{-1}(\mathbf{k}) = 2J_2 \cos(2\mathbf{k} \cdot \mathbf{a}_1 - \mathbf{k} \cdot \mathbf{a}_2) + 2J_2' \cos(-\mathbf{k} \cdot \mathbf{a}_1 + 2\mathbf{k} \cdot \mathbf{a}_2) - 2i\delta \sin(-\mathbf{k} \cdot \mathbf{a}_1 + 2\mathbf{k} \cdot \mathbf{a}_2)$.

The column μ_α of such a unitary matrix U construct the general Bogoliubov wave functions $\Psi_{1,\alpha} \equiv C_{1,\alpha} \begin{bmatrix} (A + \omega_\alpha I)\mu_\alpha \\ -B^\dagger \mu_\alpha \end{bmatrix} \equiv \begin{bmatrix} U_{1,\alpha} \\ V_{1,\alpha} \end{bmatrix}$ and $\Psi_{3,\alpha} \equiv C_{3,\alpha} \begin{bmatrix} -B\mu_\alpha \\ (A + \omega_\alpha I)\mu_\alpha \end{bmatrix} \equiv \begin{bmatrix} U_{3,\alpha} \\ V_{3,\alpha} \end{bmatrix}$ of the α -mode, where ω_α^2 and ω_β^2 are also the corresponding eigenvalues of the matrix D . The para-unitary matrix U enables $h_0 = l \cosh \vartheta$, $f_1(\mathbf{k}) = l \sinh \vartheta e^{-i\varphi}$, $f_2(\mathbf{k}) = l \sinh \theta e^{-i\phi}$ and $g_\chi(\mathbf{k}) = l \cosh \theta e^{i\zeta}$. The magnon operators $\Psi_{\mathbf{k}} = U \psi_{\mathbf{k}}$ satisfy the generalized orthonormal condition $\langle \langle \Psi_m | \Psi_n \rangle \rangle = \Psi_m^\dagger (\sigma_0 \otimes \tau_z) \Psi_n$. We rewrite our Hamiltonian in (k_x, y) space along the y direction.

$$\begin{aligned} \alpha_{ky}^\dagger &= \frac{1}{\sqrt{N_x}} \sum_m e^{ik\mathbf{R}_m \cdot \mathbf{e}_x} \alpha_{my}^\dagger, \\ \beta_{ky}^\dagger &= \frac{1}{\sqrt{N_x}} \sum_m e^{ik\mathbf{R}_m \cdot \mathbf{e}_x} \beta_{my}^\dagger. \end{aligned} \quad (\text{A-7})$$

For the anisotropic edge modes, we also give the Hamiltonian for (x, k_y) space

$$\begin{aligned} \alpha_{kx}^\dagger &= \frac{1}{\sqrt{N_y}} \sum_m e^{ik\mathbf{R}_m \cdot \mathbf{e}_y} \alpha_{mx}^\dagger, \\ \beta_{kx}^\dagger &= \frac{1}{\sqrt{N_y}} \sum_m e^{ik\mathbf{R}_m \cdot \mathbf{e}_y} \beta_{mx}^\dagger, \end{aligned} \quad (\text{A-8})$$

where y or x runs from i_1 to $4(W-1)+i_1$ ($i_1 = \{1, 2, 3, 4\}$) and W denotes the number of periodic 1D chains. We can replace k_x or k_y by k . The formalism for calculating

the band structure of the ribbon geometry is a $4W \times 4W$ matrix-form Hamiltonian which is given by

$$\mathcal{H} = \sum_{\mathbf{k}} \psi_{\mathbf{k}}^\dagger H(\mathbf{k}) \psi_{\mathbf{k}}. \quad (\text{A-9})$$

The Hamiltonian matrix can be written as

$$H(\mathbf{k}) = \begin{bmatrix} G_1(k) & F(k)^\dagger & 0 & \cdots & 0 \\ F(k) & G(k) & F(k)^\dagger & \ddots & \vdots \\ 0 & F(k) & \ddots & \ddots & 0 \\ \vdots & \ddots & \ddots & \ddots & F(k)^\dagger \\ 0 & \cdots & 0 & F(k) & G_2(k) \end{bmatrix}, \quad (\text{A-10})$$

where $G(k)$, $G_1(k)$, $G_2(k)$ and $F(k)$ are 4×4 matrices with zigzag edge states along the k_x direction and arm-chair edge states along the k_y direction. We choose $W=20$ to ensure that the results are convergent with W . To calculate the transport properties of magnons, we introduce the retarded and advanced Green's functions.

$$G^R(r, r') = \sum_{k,n} \frac{\psi_{k,n}^\dagger(r') \psi_{k,n}(r)}{\omega + i\eta - H}, \quad (\text{A-11})$$

$$G^A(r, r') = [G^R(r, r')]^\dagger,$$

where η is a positive infinitesimal, ω is the excitation energy, r and r' represent excitation and response respectively. The spectral representation of the Green's function and the magnon DOS can be written as

$$\begin{aligned} A(\omega) &= \sum_{k,n} \psi_{k,n}(r) \psi_{k,n}^\dagger(r') \frac{2\eta}{(\omega - H)^2 + \eta^2}, \\ D(\omega) &= \frac{\hbar \text{Tr}[A(\omega)]}{2\pi}. \end{aligned} \quad (\text{A-12})$$

Appendix B: Topological band structure

We derive the Berry connection $\mathbf{A}_n = i[(\sigma_0 \otimes \tau_z)U^\dagger (\sigma_0 \otimes \tau_z)\nabla U]$, which is related to the redefined inner product of BdG Hamiltonian $\langle \langle \Psi_m | \Psi_n \rangle \rangle$. Enabling a more practical form $i(\sigma_0 \otimes \tau_z)_{nn} \sum_m (\sigma_0 \otimes \tau_z)_{mm} \langle \langle \nabla \Psi_n | \Psi_m \rangle \rangle \times \langle \langle \Psi_m | \nabla \Psi_n \rangle \rangle$ of Berry curvature $\Omega_n = \nabla \times \mathbf{A}_n$.

$$\begin{aligned} \Omega_n &= i(\sigma_0 \otimes \tau_z)_{nn} \sum_{m \neq n} (\sigma_0 \otimes \tau_z)_{mm} \\ &\quad \frac{\langle \langle \Psi_n | \nabla H_k | \Psi_m \rangle \rangle \times \langle \langle \Psi_m | \nabla H_k | \Psi_n \rangle \rangle}{(E_n - E_m)^2}. \end{aligned} \quad (\text{B-1})$$

We calculate the Berry phase of half Brillouin zone that is given by $\Upsilon_n = \text{Im} \ln[\langle \langle \Psi_n(\mathbf{R}_0) | \Psi_n(\mathbf{R}_1) \rangle \rangle \dots \langle \langle \Psi_n(\mathbf{R}_{N-1}) | \Psi_0(\mathbf{R}_1) \rangle \rangle]$ via the Wilson loop method.

In weak topological phase, the transverse current is understood as a consequence of the presence of chiral edge

states induced by the δ term. We derive the magnon Hall conductivity from $\sum_n c_1[n_B(\omega)]$ by the approximation as

$$\begin{aligned} & \frac{1}{e^{\frac{\sqrt{\Lambda_\delta + \lambda_\delta}}{2k_B T}} - 1} - \frac{1}{e^{\frac{\sqrt{\Lambda_\delta - \lambda_\delta}}{2k_B T}} - 1} \\ &= \frac{\Delta^+ - \Delta^-}{2 \sinh \frac{\sqrt{\Lambda_\delta + \lambda_\delta}}{2k_B T} \sinh \frac{\sqrt{\Lambda_\delta - \lambda_\delta}}{2k_B T}}, \end{aligned} \quad (\text{B-2})$$

where k_B is the Boltzmann constant and T is the temperature. Thus, we derive Δ^+ and Δ^- to highlight the differences in altermagnetic magnons

$$\begin{aligned} \Delta^+ &= (1 + \sqrt{\Lambda_\delta + \lambda_\delta}) \sinh \frac{\sqrt{\Lambda_\delta - \lambda_\delta}}{2k_B T} \cosh \frac{\sqrt{\Lambda_\delta + \lambda_\delta}}{2k_B T}, \\ \Delta^- &= (1 + \sqrt{\Lambda_\delta - \lambda_\delta}) \sinh \frac{\sqrt{\Lambda_\delta + \lambda_\delta}}{2k_B T} \cosh \frac{\sqrt{\Lambda_\delta - \lambda_\delta}}{2k_B T}. \end{aligned} \quad (\text{B-3})$$

We choose the lattice constant $a=0.1\text{nm}$ as the typical layer spacing for practical calculation. Considering the thermal fluctuation, we calculate the deviation of sublattice magnetization from the saturation value

$$\Delta m = S - \langle S_m^z \rangle = \langle \psi_m^\dagger \psi_m \rangle = \sum_{n, \mathbf{k}} n_B(n, \mathbf{k}). \quad (\text{B-4})$$

The Curie temperature T_c is determined by $\Delta m(T_c) = S$.

The density of \mathbf{M} operator written in real space, $\mathbf{M}(\mathbf{r}) = \frac{1}{2} \Psi_r^\dagger \mathbf{M} \Psi_r$, satisfies the commutation relation $\mathbf{M} \sigma_0 \otimes \tau_z H - H \sigma_0 \otimes \tau_z \mathbf{M} = 0$. We obtain the location of

Weyl points as the zero points of the function $\lambda_1(\mathbf{k})$ along the high symmetry axis $\Gamma\text{-}\mathbf{M}^\pm$ shown in Fig. 1

$$\begin{aligned} \lambda_1(\mathbf{k}) &= 2(J_1^2 - 6J_1J_2 - 4J_2J_2' - 4J_2'^2) \cos(-\mathbf{k} \cdot \mathbf{a}_1 + 2\mathbf{k} \cdot \mathbf{a}_2) \\ &\quad + 2(J_1^2 - 6J_1J_2' - 4J_2J_2' - 4J_2'^2) \cos(2\mathbf{k} \cdot \mathbf{a}_1 - \mathbf{k} \cdot \mathbf{a}_2). \end{aligned} \quad (\text{B-5})$$

The orbital motion of a magnon wave packet is defined as the topological angular momentum without a mass term $\langle \mathbf{r} \times \mathbf{v} \rangle$, where $v_x = \sqrt{3}v_0$, $v_y = 3v_0$, and

$$\begin{aligned} v_0 &= [4(J_2J_2' + J_2^2\eta) - J_1^2] \sqrt{1 - \eta^2} \\ &\quad + 2\sqrt{(J_1^2 - h_0J_2)^2(1 - \eta^2) + \delta^2(h_0^2 - 2J_1^2 - 2J_1^2\eta)}. \end{aligned} \quad (\text{B-6})$$

We calculate the angular momentum of topological magnons along the integral form of ω by summing the edge current and the self-rotation of magnon wave packet

$$\begin{aligned} L_{self} &= m^* \sum_n \int d\omega n_B(\omega) \chi \mathbf{L}_{self}(\omega), \\ L_{edge} &= m^* \sum_n \int d\omega (TD(\omega) - \omega) n_B(\omega) \chi \Omega_\chi(\omega). \end{aligned} \quad (\text{B-7})$$

In Fig. 5, we have focused on the interplay between the magnon altermagnet and the Berry curvature, which have opposite signs between the two Weyl points, resulting in an intrinsic magnon spin Hall current.